

# PCCP

Physical Chemistry Chemical Physics

Accepted Manuscript

This article can be cited before page numbers have been issued, to do this please use: H. F. Zhao, L. Franzon, S. Juttula, R. E. N. Skog, N. Myllys and T. Kurtén, *Phys. Chem. Chem. Phys.*, 2026, DOI: 10.1039/D5CP04635A.



This is an Accepted Manuscript, which has been through the Royal Society of Chemistry peer review process and has been accepted for publication.

Accepted Manuscripts are published online shortly after acceptance, before technical editing, formatting and proof reading. Using this free service, authors can make their results available to the community, in citable form, before we publish the edited article. We will replace this Accepted Manuscript with the edited and formatted Advance Article as soon as it is available.

You can find more information about Accepted Manuscripts in the [Information for Authors](#).

Please note that technical editing may introduce minor changes to the text and/or graphics, which may alter content. The journal's standard [Terms & Conditions](#) and the [Ethical guidelines](#) still apply. In no event shall the Royal Society of Chemistry be held responsible for any errors or omissions in this Accepted Manuscript or any consequences arising from the use of any information it contains.

Cite this: DOI: 00.0000/xxxxxxxxxx

# Clustering effects on the reactivity of alkoxy radicals: Rate coefficients of ${}^3(\text{RO}\cdots\text{OR})$ complexes accounting for multiple conformers<sup>†</sup>

Hongye Fraise Zhao<sup>a</sup>, Lauri Franzon<sup>a</sup>, Severi Juttula<sup>a</sup>, Robert Skog<sup>a</sup>, Nanna Mylly<sup>a</sup> and Theo Kurtén<sup>a</sup>

Received Date  
Accepted Date

DOI: 00.0000/xxxxxxxxxx

Atmospheric peroxy ( $\text{RO}_2^*$ ) and alkoxy ( $\text{RO}^*$ ) radical species are crucial intermediates in the formation of secondary organic aerosol (SOA). Recent computational work has demonstrated that recombination reactions of peroxy radicals ( $\text{RO}_2^* + \text{RO}_2^*$ ) proceed through triplet complexes consisting of two alkoxy radicals ( ${}^3(\text{RO}\cdots\text{OR})$ ). To understand how peroxy recombination reactions branch into different product channels, it is thus necessary to thoroughly investigate the reactions of these triplet alkoxy complexes. Although the reactions of free alkoxy radicals have been extensively studied, the reactivity of triplet alkoxy complexes remains relatively less explored. In this study, we have therefore developed a systematic conformer sampling workflow for  ${}^3(\text{RO}\cdots\text{OR})$ , and applied it to four typical alkoxy systems (AceO,  $\beta$ -ISOPO,  $\text{PhCH}_2\text{O}$ , and  $\text{PhC}(\text{O})\text{O}$ ). Rate coefficients ( $k$ ) of key reactions have been calculated using multi-conformer and lowest-conformer transition state theory (MC-TST and LC-TST), allowing the quantitative evaluation of conformer effects. Our results demonstrate that the presence of the other  $\text{RO}^*$  in the complex has a noticeable effect on  $k$  values. For the  $\beta$ -ISOPO system in particular, the predicted  $\beta$ -scission  $k$  values in the  ${}^3(\text{RO}\cdots\text{OR})$  complex are over 100 times higher than for the free radical.

## 1 Introduction

Climate change and air pollution have become major challenges in current times. As a pollutant, small atmospheric particles account for around 10 million global deaths and  $10^8$  disability-adjusted life years annually.<sup>1,2</sup> On the other hand, atmospheric aerosols can cool the climate through cloud formation and scattering.<sup>3</sup> Sustainable development actions have significantly reduced the emission of inorganic species (e.g.  $\text{NO}_x$ ,  $\text{SO}_2$ , etc.), initiating a shift in aerosol compositions: Before those actions, atmospheric aerosols were dominated by primary inorganic aerosols; afterwards, secondary organic aerosol (SOA) particles have become more influential<sup>4</sup>.

A major source of SOA is volatile organic compounds (VOCs), which come from various biogenic (e.g. isoprene molecules released by vegetation)<sup>5</sup> and anthropogenic (e.g. fuel combustion, usage of organic solvents)<sup>6</sup> emissions. After emission, VOCs are oxidized and converted into peroxy radicals ( $\text{RO}_2^*$ ). Depending on its molecular structure,  $\text{RO}_2^*$  can undergo both unimolecular

reactions, such as H-shifts and ring closures, and bimolecular reactions with species including  $\text{NO}_x$ ,  $\text{HO}_x$  and  $\text{RO}_2^*$ .<sup>7</sup> Among these channels, we are especially interested in the peroxy recombination reaction (R1 in Figure 1), as some subsequent channels can generate accretion products<sup>8</sup> (e.g. R2.3 and R2.4 in Figure 1), which are critical for SOA formation. Compared to the initial VOCs, accretion products have a higher number of carbon atoms and lower volatility<sup>9</sup>, allowing them to cluster very efficiently.

As shown in Figure 1, the peroxy recombination reaction proceeds via a tetroxide intermediate, and generally<sup>1</sup> leads to a triplet alkoxy complex ( ${}^3(\text{RO}\cdots\text{OR})$ ) after releasing one  ${}^3\text{O}_2$  molecule.<sup>11,12</sup> The  ${}^3(\text{RO}\cdots\text{OR})$  complex consists of two alkoxy radicals ( $\text{RO}^*$ ) and can undergo various reactions. Therefore, the branching of peroxy recombination channels reflects different fates of  ${}^3(\text{RO}\cdots\text{OR})$ .

So far, four reaction channels of  ${}^3(\text{RO}\cdots\text{OR})$  have been discovered: dissociation<sup>13</sup> (R2.1 in Figure 1), intermolecular H-shift<sup>14,15</sup> (R2.2 in Figure 1), intersystem crossing (ISC)<sup>16</sup> to the singlet surface (R2.3 in Figure 1), and  $\beta$ -scission of one of the

<sup>a</sup> Department of Chemistry, University of Helsinki, A.I. Virtasen aukio 1 (Chemicum), 00560, Helsinki, Finland. Tel: +358 (0)294150289; E-mail: theo.kurten@helsinki.fi

<sup>†</sup> Supplementary Information available: Further discussions are included in the SI document (DOI: 10.1039/D5CP00000x/), and output files of key conformers in this study are uploaded to a Zenodo archive (DOI: 10.5281/zenodo.19210535)

<sup>1</sup> According to the experimental results of Murphy et al.<sup>10</sup>, for certain peroxy radicals such as  $\text{HOCH}_2\text{CH}_2\text{OO}^*$ , the recombination reaction might also proceed through a  ${}^1(\text{RO}\cdots\text{O}_2\cdots\text{OR})$  complex and produce  $\text{HO}_2^*$ . The reaction can be summarized as follows:  $\text{RO}_2^* + \text{RO}_2^* \rightarrow {}^1(\text{RO}\cdots\text{O}_2\cdots\text{OR}) \rightarrow \text{R-H}=\text{O} + \text{HO}_2^* + \text{RO}^*$ .



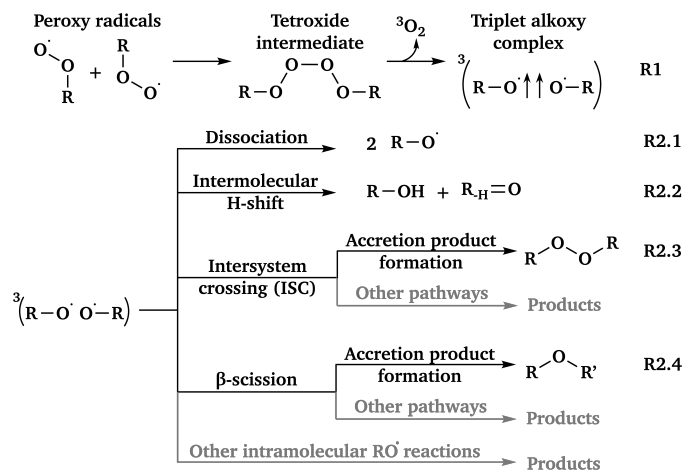


Fig. 1 The known product channels of peroxy recombination reactions.

alkoxy radicals<sup>17,18</sup> (R2.4 in Figure 1). Rate coefficients ( $k$ ) reported for these channels vary widely with both the structure of the  $^3(\text{RO}\cdots\text{OR})$  and the calculation method. Nevertheless, all four channels share a common feature: They can proceed very rapidly, with estimated  $k(298\text{ K})$  values often exceeding  $10^9\text{ s}^{-1}$ .<sup>14,15,17</sup>

In addition to  $\beta$ -scissions, other intramolecular reactions may also take place depending on the structure of the reactive  $\text{RO}\cdot$ . These intramolecular reactions include  $\text{CO}_2$  elimination in acyloxy radicals<sup>19</sup>, intramolecular H-shifts<sup>20,21</sup> and epoxide formation<sup>22,23</sup>. We expect that any sufficiently fast intramolecular  $\text{RO}\cdot$  reaction<sup>24</sup> can also occur in  $^3(\text{RO}\cdots\text{OR})$  — but the in-complex rate is likely to differ from that of the free-radical reaction.

Among the reaction channels of  $^3(\text{RO}\cdots\text{OR})$ , ISC and  $\beta$ -scission are of special importance, as they may lead to recombination processes that form accretion products. In general, the ester or ether products from  $\beta$ -scission ( $\text{ROR}'$ ) are expected to be more stable, and therefore longer-lived, than the peroxide products from ISC ( $\text{ROOR}$ ).<sup>17</sup> However, note that neither ISC nor  $\beta$ -scission reactions guarantee the accretion product formation, as other competing processes may intervene before recombination. For example, H-shift and dissociation reactions can take place in  $^1(\text{RO}\cdots\text{OR})$  (from ISC)<sup>25</sup> or  $^3(\text{R}'\cdots\text{OR}\cdots\text{CH}_2\text{O})$  (from  $\beta$ -scission) complexes. Additionally, the  $\text{ROR}'$  formation after  $\beta$ -scission probably requires a subsequent ISC.<sup>17</sup>

Given the importance of atmospheric  $^3(\text{RO}\cdots\text{OR})$  complexes, a natural progression is to investigate the rate coefficients of their different reactions. Numerous experimental studies have probed the final product distribution of peroxy radical recombination. For example, Frandsen et al.<sup>18</sup> recently studied the ozonolysis of tetramethylethylene (TME), where the dominant first-generation  $\text{RO}_2\cdot$  is the acetyl peroxy radical,  $\text{CH}_3\text{C}(\text{O})\text{CH}_2\text{OO}\cdot$  ( $\text{AceOO}\cdot$ ). Products with the elemental composition  $\text{C}_6\text{H}_{10}\text{O}_4$  were abundantly observed, suggesting ISC as the major channel. On the other hand, Peräkylä et al.<sup>17</sup> detected  $\text{C}_{19}$  esters as the primary accretion product of  $\alpha$ -pinene ( $\text{C}_{10}$ ) ozonolysis, implying that  $\beta$ -scission dominates the accretion product formation.

Although experiments can probe the final product distribu-

tion of  $\text{RO}_2 + \text{RO}_2$  reactions, and even have recently captured the tetroxide intermediate in the gas phase (observed as  $\text{R}_2\text{O}_4(\text{H}_2\text{O})\text{H}^+$ )<sup>26</sup>, current techniques are still unable to detect the  $^3(\text{RO}\cdots\text{OR})$  directly, as this complex is too short-lived for spectroscopic detection or isolation. Alternatively, theoretical methods can reveal the structures of key intermediates and estimate the stepwise reaction rates.

Previous theoretical studies<sup>14,15</sup> have shown the difficulties of studying the in-complex reactions: (1) The  $^3(\text{RO}\cdots\text{OR})$  complex, an open-shell species with two unpaired electrons, is different from the benchmarking species used by major computational chemistry methods, up to and including state-of-the-art methods such as coupled cluster. It is noteworthy that the training sets of xTB methods, which are commonly used for semi-empirical conformer sampling, are primarily closed-shell species.<sup>27–29</sup> (2) The structural variety of  $^3(\text{RO}\cdots\text{OR})$  conformers affects the accuracy of predicted thermodynamic and kinetic parameters. By definition, each conformer corresponds to a distinct potential energy minimum<sup>30</sup>. Energetically low-lying conformers influence the rate coefficient as their Boltzmann population is non-zero.<sup>31,32</sup> Previous computational studies have suggested that ignoring conformers other than the global minimum may lower the accuracy of the rate coefficient prediction, especially at higher temperatures relevant to combustion.<sup>31,33</sup> Furthermore, compared to  $\text{RO}\cdot$ , a larger number of conformers can be expected for  $^3(\text{RO}\cdots\text{OR})$  due to intermolecular interactions.

Based on the discussions above, to compute the reaction rate coefficients of  $^3(\text{RO}\cdots\text{OR})$  more accurately, a systematic conformer search workflow is required. In this study, we improve the conformer sampling workflow reported by Hasan et al.<sup>14,15</sup> and Møller et al.<sup>31</sup>, with a special focus on intermolecular H-shift reactions. Since these reactions involve both  $\text{RO}\cdot$  in the  $^3(\text{RO}\cdots\text{OR})$  complex and certain computational tools (e.g. GOAT) had not been developed at that time, previous studies<sup>14,15</sup> encountered challenges to sample the transition state (TS) conformers of intermolecular H-shift reactions comprehensively. Then, we apply our updated workflow to four  $^3(\text{RO}\cdots\text{OR})$  systems corresponding to representative  $\text{RO}_2\cdot + \text{RO}_2\cdot$  pairs in the atmosphere. We determine the  $k$  values of  $\beta$ -scission, intermolecular H-shift and other selected reactions, such as  $\text{RO}\cdot$  addition to a double bond (R3.2.2(a)-(b) in Figure 3) and epoxy formation-decomposition (R3.3.2 (1)-(2) in Figure 4). In addition to investigating the relevance of these novel pathways, our main purpose is to assess how clustering with another  $\text{RO}\cdot$  affects the reactivity of alkoxy radicals, which is achieved by comparing the free-radical and in-complex  $k$  values.

This study does not include the rate coefficients of dissociation and ISC channels. For the dissociation channel,  $k$  strongly depend on the binding energy ( $D$ ) of the  $^3(\text{RO}\cdots\text{OR})$ <sup>13</sup>, and the  $D$  values are reported in Table S2 of the Supplementary information (SI) (with relevant notations defined in Table S1). For the ISC channel, determining both the ISC rate and the post-ISC product distribution require additional calculations on the highly multireference open-shell singlet surface, which is beyond the scope of this work.

The names and  $\text{RO}\cdot$  molecular formulas of the four systems are



listed in Table 1. Each system includes both free radicals and triplet complexes. The simplified notations for  $^3(\text{RO}\cdots\text{OR})$  are similar to their corresponding  $\text{RO}\cdot$ .

These four systems were selected based on experimental evidence and atmospheric importance:  $\text{AceO}\cdot$  can be formed in tetramethylethylene (TME) ozonolysis, and several experimental studies<sup>18,34,35</sup> have investigated its product distribution.  $\beta\text{-ISOPO}\cdot$ , as the name implies, can be generated in the  $\cdot\text{OH}$ -oxidation processes of isoprene<sup>36</sup>. Since stereochemistry is not the focus of this study, we selected only (*S*)-enantiomers of the  $\beta\text{-ISOPO}\cdot$  for simplicity.  $\text{PhC}(\text{O})\text{O}\cdot$  and  $\text{PhCH}_2\text{O}\cdot$  were selected as representative aromatic alkoxy radicals as they are formed during the oxidation of toluene. In brief,  $\text{Cl}\cdot$ ,  $\cdot\text{OH}$  or  $\text{NO}_3\cdot$  initiate a methyl H-abstraction reaction from toluene,<sup>37</sup> followed by  $\text{O}_2$  addition to form  $\text{PhCH}_2\text{OO}\cdot$ . Recombination reactions of  $\text{PhCH}_2\text{OO}\cdot$  then generate the corresponding alkoxy radical,  $\text{PhCH}_2\text{O}\cdot$ , as well as benzaldehyde ( $\text{PhCHO}$ ).<sup>38</sup> Subsequently,  $\text{PhCHO}$  can be oxidized into  $\text{PhC}(\text{O})\text{O}\cdot$ .<sup>39</sup>

## 2 Computational details

### 2.1 Notations and computational chemistry programs applied in this study

For clarity and succinctness, Table 2 summarizes the simplified notations of the types of reactants and transition states, computational methods and energy terms used in this study. Detailed discussions of computational methods are provided in Sections 2.2 – 2.4. A schematic representation of the conformer sampling workflow is reported in Figure S1.

The initial structures of isolated  $\text{RO}\cdot$  were built in SPARTAN<sup>24</sup>.<sup>40</sup> Reactant and transition state (TS) dimers were generated using the artificial bee colony algorithm for cluster global optimization (ABCluster) 3.3 program<sup>41,42</sup>. Transition state structures of intermolecular H-shift reactions (TS H-shift) were generated using the global optimization algorithm (GOAT)<sup>43</sup> implemented in ORCA 6.0.1<sup>44</sup>. Semi-empirical calculations were performed using XTB 6.7.1<sup>45,46</sup>. Calculations at higher level of theories, including density functional theory (DFT) and coupled cluster methods, were performed with ORCA 6.0.1<sup>44</sup>. Filtering and analysis of the results were done using the Jammy Key for Configurational Sampling (JKCS) 2.1 program<sup>47–49</sup>.

### 2.2 Method for rate coefficient calculation and relevant energy barriers

Earlier studies reported that  $\beta$ -scission and intermolecular H-shift reactions of  $^3(\text{RO}\cdots\text{OR})$  proceed through a single transition state<sup>14,15</sup>, and can thus be treated as elementary reactions<sup>50</sup>. In addition, reactions taking place within a  $^3(\text{RO}\cdots\text{OR})$  complex do not involve collisions or exchanges with other molecular entities, and can therefore be treated as unimolecular elementary reactions. These reactions are further categorized as follows: If the reaction involves only one  $\text{RO}\cdot$  in the  $^3(\text{RO}\cdots\text{OR})$  complex, it is a unimolecular intramolecular reaction. In contrast, if the reaction involves both  $\text{RO}\cdot$  in the complex, it is a unimolecular intermolecular reaction. The first category includes  $\beta$ -scission, epoxy formation and decomposition, while the second category

includes intermolecular H-shift and  $\text{RO}\cdot$  addition to the double bond.

Therefore, reaction rate coefficients in this study are calculated using the elementary transition state theory (TST)<sup>51,52</sup>. Although absolute  $k$  values predicted by elementary TST are often inaccurate, the relative rates are more reliable (e.g. the  $\frac{k(\beta\text{-scission, in-complex})}{k(\beta\text{-scission, free-radical})}$  factor, which is further discussed in Section 3.5.). In addition, according to Hasan et al.<sup>14</sup>, variational effects are unlikely to be a major source of error even for rapid reactions in alkoxy complexes. The difference between their H-shift rate coefficients computed using elementary and variational TST are generally within a factor of two<sup>14</sup>, suggesting that elementary TST is capable of describing such systems, and consequently, sufficient for this study.

In practice, elementary TST is applied in two forms when calculating  $k$ <sup>31</sup>: multi-conformer TST (MC-TST)<sup>31,53</sup>, which accounts for contributions from multiple conformers (within an energy cut-off) in Equation 1; or lowest-conformer TST (LC-TST)<sup>31</sup>, which includes only the conformer with the lowest (free) energy value, and thus with the highest Boltzmann probability, in Equation 2.

$$k(\text{MC-TST}) = \kappa_{\min} \frac{k_{\text{B}}T}{h} \frac{\sum_i^{n_{\text{TS}}} \exp\left(-\frac{G_{\text{TS}_i} - G_{\text{R}_{\min}}}{RT}\right)}{\sum_j^{n_{\text{R}}} \exp\left(-\frac{G_{\text{R}_j} - G_{\text{R}_{\min}}}{RT}\right)} \quad (1)$$

$$k(\text{LC-TST}) = \kappa_{\min} \frac{k_{\text{B}}T}{h} \exp\left(-\frac{G_{\text{TS}_{\min}} - G_{\text{R}_{\min}}}{RT}\right) \quad (2)$$

In Equations 1 and 2,  $\kappa_{\min}$  is the tunneling coefficient,  $T$  is the temperature,  $k_{\text{B}}$  is the Boltzmann constant,  $h$  is the Planck constant,  $R$  is the gas constant,  $G_{\text{TS}}$  is the Gibbs free energy value of the transition state and  $G_{\text{R}}$  is the the Gibbs free energy value of the reactant. The subscripts indicate the following information: "min" is for the lowest-energy conformer, "i" is for any TS conformer, and "j" is for any reactant conformer.

As Møller et al.<sup>31</sup> reported, one  $\kappa$  value is often sufficient to represent the tunneling effect for all conformers of the same reaction. This coefficient corresponds to the tunneling coefficient of the lowest-energy TS conformer<sup>31</sup>, denoted  $\kappa_{\min}$ . In practice, the  $\kappa_{\min}$  value was calculated using the Eckart tunneling method<sup>54</sup>, which requires the forward and backward barrier heights and imaginary frequency ( $\omega_i$ ) of the TS on the potential energy surface (PES). The PES was obtained with the intrinsic reaction coordinate (IRC)<sup>55</sup> approach in ORCA 6.0.1. The IRC endpoints were then optimized, and their zero-point corrected electronic energy ( $E_{\text{elzpc}}$ ) values were used to compute the barrier heights for the  $\kappa_{\min}$  calculation.<sup>31,32</sup>

### 2.3 Conformer sampling of free-radical reactions

For each reaction channel, a single  $\text{RO}\cdot$  structure (reactant monomer) from SPARTAN was optimized at two density functional theory (DFT) levels in ORCA: first at the B3LYP<sup>56,57</sup>/ma-def2-SVP<sup>58,59</sup> level, and then at the  $\omega\text{B97X-D3}$ <sup>60,61</sup>/ma-def2-TZVP<sup>58,59</sup> level. The choice of B3LYP and  $\omega\text{B97X-D3}$  functionals is suggested by previous studies on  $^3(\text{RO}\cdots\text{OR})$  complexes<sup>14,15,17,21</sup>, as well as benchmarking work on general chem-



**Table 1** Systems involved in this study, and the names used to refer to them throughout this paper.

Simplified notation in this paper	Full name	Molecular formula of RO <sup>•</sup>	Structure of RO <sup>•</sup>
AceO radical or AceO <sup>•</sup>	Acetyl alkoxy radical	C <sub>3</sub> H <sub>5</sub> O <sub>2</sub>	
β-ISOPO radical or β-ISOPO <sup>•</sup>	(S)-1-methyl-1-vinyl-2-hydroxyethyl alkoxy radical	C <sub>5</sub> H <sub>9</sub> O <sub>2</sub>	
PhCH <sub>2</sub> O radical or PhCH <sub>2</sub> O <sup>•</sup>	Benzyl alkoxy radical	C <sub>7</sub> H <sub>7</sub> O	
PhC(O)O radical or PhC(O)O <sup>•</sup>	Benzyl acyloxy radical	C <sub>7</sub> H <sub>5</sub> O <sub>2</sub>	

ical databases<sup>62</sup> and atmospheric molecular clusters<sup>63</sup>. Tests of different basis sets on <sup>3</sup>(AceO<sup>•</sup> ··· OAce)<sup>64</sup> and small gas-phase clusters<sup>65</sup> indicate that ma-def2-SVP and ma-def2-TZVP basis sets are sufficiently accurate for the systems studied in this paper with good computational efficiency.

After optimization at the B3LYP level, the reactant monomer was optimized at the ωB97X-D3 level in two subsequent steps: first with the default grid size (no additional keywords required, or specified by the keyword "DefGrid2")<sup>44,66</sup> and then with the largest predefined grid size in ORCA 6.0.1 (invoked by the keyword "DefGrid3")<sup>66,67</sup>. These two steps at ωB97X-D3 level will be referred to as "ωB97X-D3 (Grid2)" and "ωB97X-D3 (Grid3)" throughout this paper. Grid3 was applied to eliminate the imaginary frequencies caused by numerical noise<sup>68</sup>. If there were still small imaginary frequencies after optimizations with Grid3, approaches such as subtle displacement along the vector or applying tighter convergence criteria would be applied.

The TS monomer was determined by relaxed surface scans at the B3LYP level of theory. The TS structure from scans were then optimized at B3LYP, ωB97X-D3 (Grid2) and ωB97X-D3 (Grid3) levels, similar to its corresponding reactant monomer.

Based on the optimized reactant and TS monomer structures, conformer searches were performed using GOAT with the GFN2-xTB<sup>28,45</sup> method in ORCA, with an energy cutoff of 15 kcal mol<sup>-1</sup>. Conformers generated by GOAT were then optimized at the B3LYP level, followed by filtering based on their uniqueness and relative energy values. Detailed selection criteria are:

- Any two selected conformers must differ by more than 0.01 Å in gyration radius ( $\Delta R_g > 0.01$ ), 0.001 Hartree in electronic energy ( $\Delta E_{el} > 0.001$  Hartree), and 0.1 Debye in dipole moment ( $\Delta p > 0.1$  Debye)<sup>14,49</sup>. This criterion, which is also the default setting in JKCS 2.1, will hereafter be referred to as the "uniqueness filter" or "filtered by uniqueness".
- The Gibbs free energy value of every selected conformer must be no more than 5 kcal mol<sup>-1</sup><sup>14,31</sup> above the global minimum ( $G - G_{\min} < 5$  kcal mol<sup>-1</sup>). This criterion will be referred to as " $G_{\text{cutoff}} = 5$  kcal mol<sup>-1</sup>" hereafter. Other

energy-based filters will also be written in the form of " $E_{\text{energy type, cutoff}} = x$  kcal mol<sup>-1</sup>".

B3LYP-optimized and filtered conformers were further optimized at the ωB97X-D3 (Grid2) level, and the optimized structures were filtered by uniqueness. Following this, the conformers were optimized at the ωB97X-D3 (Grid3) level, and then filtered by uniqueness and  $G_{\text{cutoff}} = 2$  kcal mol<sup>-1</sup>.

Conformers satisfying all the criteria discussed above were forwarded to the next step. To improve the accuracy of relative energy predictions, single-point energy calculations on top of the ωB97X-D3 (Grid3) optimized structures were performed using the following coupled cluster method: UHF<sup>69</sup>-DLPNO-CCSD(T)<sup>70</sup>-F12<sup>71</sup>/cc-pVDZ-F12<sup>72</sup>, with the keyword "tightPNO"<sup>73</sup> and "tightSCF", cc-pVDZ-F12-CABS<sup>72</sup> as the auxiliary basis set, and aug<sup>74</sup>-cc-pVDZ<sup>75</sup>/C as the RI approximation basis set. This method was suggested by our benchmarking results and previous studies on atmospheric molecular clusters<sup>63,76</sup>. Coupled cluster calculations were only carried out on lowest-energy conformers ( $G_{\min}$ ), as suggested by previous studies<sup>14,15,31,32</sup>.

Following the DLPNO-CCSD(T)-F12 calculations, energy corrections were computed as  $E_{\text{sp}}(\text{CCSD(T)}) - E_{\text{el}}(\text{DFT})$  for the lowest-energy reactant and TS monomers, respectively, and applied to other conformers of the same type. The coupled cluster-corrected  $G_R$  and  $G_{\text{TS}}$  values were applied to calculate the  $k(\text{CC})$  of free-radical reactions.

Finally,  $k(\text{DFT})$  and  $k(\text{CC})$  were computed using both MC-TST (Equation 1) and LC-TST (Equation 2) methods to evaluate the effects of coupled-cluster corrections and contributions from multiple conformers. Consequently, four  $k$  values were reported for each reaction channel.

## 2.4 Conformer sampling of in-complex reactions

### 2.4.1 Conformer sampling of reactant dimers

Based on the reactant monomers from Section 2.3, reactant dimers were generated using ABCluster 3.3, executed through JKCS2.1. Monomers were treated rigidly (i.e. with fixed internal coordinates)<sup>42</sup> and placed against each other with a CHARMM36<sup>77,78</sup>-based force field. ABCluster requires three types of input data<sup>41,42</sup>: monomer coordinates (in .xyz format), atom-wise partial charges and force field parameters ( $\epsilon$  and  $\sigma$ ). Partial charges were calculated using the natural bond orbital (NBO) 7.0.10<sup>79,80</sup> program interfaced to ORCA 6.0.1. The  $\epsilon$  and

<sup>II</sup> The conformer search will stop going uphill if  $E(\text{new conformer}) - E(\text{initial conformer}) > 15 + 3N_{\text{atom}}$  kcal mol<sup>-1</sup>, where  $N_{\text{atom}}$  is the number of atoms in the conformer. This is invoked by the keyword "MaxEn 15.0".<sup>43</sup>



**Table 2** Simplified notations of conformers, computational methods and energy terms in this study.

Simplified notation in this paper	Detailed descriptions
Reactant monomer	An isolated RO <sup>•</sup> radical.
TS monomer	A transition state conformer of intramolecular RO <sup>•</sup> reactions.
Reactant dimer	A triplet alkoxy complex, <sup>3</sup> (RO · · · OR).
TS H-shift conformer	A transition state conformer of the intermolecular H-shift reaction of <sup>3</sup> (RO · · · OR), which involves both RO <sup>•</sup> in the complex.
TS dimer	A transition state conformer of other intramolecular reaction channels of <sup>3</sup> (RO · · · OR), which takes place within one RO <sup>•</sup> of the complex.
B3LYP	B3LYP/ma-def2-SVP.
ωB97X-D3 (Grid2)	ωB97X-D3/ma-def2-TZVP, with the default grid size of ORCA 6.0.1.
ωB97X-D3 (Grid3)	ωB97X-D3/ma-def2-TZVP, with the largest predefined grid size of ORCA 6.0.1.
DLPNO-CCSD(T)-F12	UHF-DLPNO-CCSD(T)-F12/cc-pVDZ-F12, with the keyword "tightPNO" and "tightSCF", cc-pVDZ-F12-CABS as the auxiliary basis set, and aug-cc-pVDZ/C as the RI approximation basis set.
<i>f</i> (DFT)	Values calculated at the ωB97X-D3/ma-def2-TZVP (DefGrid3) level of theory, where <i>f</i> can be an energy term ( <i>E</i> ) or rate coefficient ( <i>k</i> ).
<i>f</i> (CC)	Values calculated at the UHF-DLPNO-CCSD(T)-F12/cc-pVDZ-F12 level of theory, where <i>f</i> can be <i>E</i> or <i>k</i> .
<i>E</i> <sub>el</sub>	Electronic energy
<i>E</i> <sub>elzc</sub>	Zero-point corrected electronic energy
<i>G</i>	Gibbs free energy
<i>D</i>	Dissociation energy of a complex
<i>E</i> <sub>sp</sub>	Single-point energy
Δ <sub>b</sub> <i>E</i>	The energy barrier of a reaction (Δ <sub>b</sub> <i>E</i> = <i>E</i> <sub>TS</sub> – <i>E</i> <sub>Reactant</sub> ), which reflects the kinetic feasibility of the reaction.
Δ <sub>r</sub> <i>E</i>	The reaction energy (Δ <sub>r</sub> <i>E</i> = <i>E</i> <sub>Product</sub> – <i>E</i> <sub>Reactant</sub> ), which reflects the thermodynamic feasibility of the reaction.

σ values were generated using the "topgen" module of ABCluster, and then examined and adjusted by the authors when necessary. With the input data above, ABCluster was invoked by the following command: JKCS2\_explore -pop 1280 -gen 320 -lm 100 -exploded -repeat 10. This command would guarantee that the initial number of dimers generated for each monomer combination was 1000<sup>III</sup>, as previous studies suggested<sup>15,81</sup>.

Reactant dimers were collected and optimized using the GFN1-xTB<sup>27,45</sup> method with necessary constraints. For atmospheric molecular clusters, the GFN1-xTB method was reported to have better agreement with DFT energy values than GFN2-xTB.<sup>81,82</sup> In addition, GFN1-xTB showed less problems than GFN2-xTB during the geometry optimization of alkoxy dimers. GFN1-optimized

structures were then filtered by uniqueness and *E*<sub>el, cutoff</sub> = 15 kcal mol<sup>-1</sup><sup>15</sup>.

The filtered conformers were then optimized at the B3LYP level in ORCA. Based on our benchmarking results, applying the *E*<sub>el</sub> cutoff of 5 kcal mol<sup>-1</sup> was equivalent to applying the *G* cutoff of 5 kcal mol<sup>-1</sup>. Thus, frequency calculations were omitted at this step to reduce computational cost. After B3LYP optimization, reactant dimers were filtered by uniqueness and *E*<sub>el, cutoff</sub> = 5 kcal mol<sup>-1</sup><sup>15,31</sup>.

Subsequently, reactant dimers were optimized at the ωB97X-D3 level in ORCA. Geometry optimizations and frequency calculations were first performed with Grid2 and filtered by uniqueness. Similar calculations were then performed with Grid3, with special attention to convergence and frequencies, and the final structures were filtered by uniqueness.

The reactant dimer with the lowest *G* value at the ωB97X-D3 (Grid3) level was selected for the coupled cluster calculation. Its *E*<sub>sp</sub> was calculated using the DLPNO-CCSD(T)-F12 method, and the energy correction (see Section 2.3) was applied to other reactant dimers. The coupled cluster-corrected *G* values of reactant dimers were substituted into the *G*<sub>R</sub> terms of Equations 1 and 2.

#### 2.4.2 Conformer sampling of TS H-shift conformers

As discussed in Section 2.4.1, ABCluster 3.3 requires "isolated" monomers as input to generate corresponding dimers. However, the TS H-shift conformer resembles more a connected moiety (two RO<sup>•</sup> connected through a C–H · · · O structure) rather than two separate monomers. Thus, ABCluster is not suitable for building initial TS H-shift structures. Alternatively, generation and semi-empirical optimization of TS H-shift conformers were performed using GOAT, with the GFN1-xTB method and an energy cutoff of 15 kcal mol<sup>-1</sup>.

TS H-shift conformers from GOAT were then optimized using the B3LYP method. A constrained optimization without frequency calculation was first performed. The constrained optimization step fixes the distance between the two atoms strongly involved in the TS, while relaxing and optimizing the rest part of the structure.<sup>83</sup> For the alkoxy systems studied, this step can reduce the computational cost and allow the following TS optimization to converge more easily. Each imaginary frequency was checked carefully to ensure it corresponded to the expected vibrational mode. Conformers that converged with correct vibrational modes at the B3LYP level were filtered by uniqueness and *G*<sub>cutoff</sub> = 5 kcal mol<sup>-1</sup>.

Following that, TS H-shift conformers were optimized at the ωB97X-D3 level in three steps: constrained optimization, TS optimization with Grid2, and TS optimization with Grid3. Frequencies were carefully examined, and de-noise approaches described in Section 2.3 were applied if necessary. A uniqueness filter was applied both before and after the ωB97X-D3 (Grid3) optimization.

Finally, a single point calculation of the TS H-shift conformer at the DLPNO-CCSD(T)-F12 level was performed on top of the ωB97X-D3 (Grid3) optimized structure with the lowest *G* value. Energy corrections were calculated as discussed in Section 2.3. The coupled cluster-corrected *G* values of TS H-shift conformers

<sup>III</sup> For example, if there are two conformers of AceO<sup>•</sup>, the number of possible <sup>3</sup>(AceO · · · OAce) combinations will be three, and the ABCluster step will generate 3000 initial structures of <sup>3</sup>(AceO · · · OAce).



were then substituted into the  $G_{TS}$  terms of Equations 2 and 1. Together with the  $G_R$  terms from Section 2.4.1, these values were applied to calculate the  $k(CC)$  of intermolecular H-shift reaction. In addition,  $k(DFT)$  values were also calculated as described in Section 2.3.

### 2.4.3 Conformer sampling of TS dimers

For other intramolecular reaction channels of  ${}^3(RO \cdots OR)$ , their TS conformers behave more like a complex consisting of two separate  $RO^\bullet$  moieties, similar to the reactant dimers described in Section 2.4.1. Therefore, ABCluster can be used to generate these TS dimers with suitable input (one reactant monomer and one TS monomer). Semi-empirical optimizations were performed using the GFN1-xTB method. After applying the uniqueness and  $E_{el, cutoff} = 15 \text{ kcal mol}^{-1}$  filters, TS dimers were optimized at the B3LYP level in two steps: constrained and TS optimization. Geometry convergence and frequencies were carefully examined, followed by the uniqueness and  $G_{cutoff} = 5 \text{ kcal mol}^{-1}$  filters.

After B3LYP optimizations and filtering, the TS dimers were optimized at the  $\omega B97X-D3$  level in three steps, as described in Section 2.4.2. A uniqueness filter was applied both before and after the  $\omega B97X-D3$  (Grid3) optimization. Frequencies were examined as in Section 2.4.2, and when required, de-noise approaches (see Section 2.3) were applied. Thereafter,  $E_{sp}$  were calculated at the DLPNO-CCSD(T)-F12 level, and energy corrections were applied as in Section 2.3. The coupled cluster-corrected  $G$  values of TS dimers were substituted into the  $G_{TS}$  terms of Equations 2 and 1. Together with the  $G_R$  terms from Section 2.4.1, these values were employed to compute the  $k(CC)$  of other intramolecular  ${}^3(RO \cdots OR)$  reactions. Additionally,  $k(DFT)$  values were also calculated as described in Section 2.3.

## 3 Results and discussion

This section first presents the number of conformers for each alkoxy system after sampling (Table 3) and calculated  $k$  values using different methods (Table 4). Further discussions on each system are provided in the following subsections. Multireference and spin contamination diagnostics, conformer-wise relative energy values (including conformers from sampling and IRC endpoints) and imaginary frequencies that correspond to vibrational modes of the transition state are reported in Tables S3 – S10.

### 3.1 The AceO system

Structures of key species during the  $\beta$ -scission and intermolecular H-shift reactions are shown in Figure 2. Given the relatively simple structure of  $AceO^\bullet$ , only a small number of conformers were found for the AceO system after the sampling workflow (see Table 3). Rate coefficients calculated at different levels of theory are listed in Table 4.

Table 4 and previous theoretical studies indicate that the intermolecular  $\beta$ -scission is among the fastest of the four reaction channels of  ${}^3(AceO \cdots OAc)$ : Its rate coefficient ( $10^9 - 10^{10} \text{ s}^{-1}$ ) exceeds that of the intermolecular H-shift ( $10^5 - 10^7 \text{ s}^{-1}$ , this study) and ISC ( $4 \times 10^8 \text{ s}^{-1}$ <sup>14,16</sup>) reactions, and is comparable to that of dissociation ( $1.5 \times 10^9 \text{ s}^{-1}$ <sup>13</sup>). Moreover, for all four methods employed to compute  $k$  values, the presence of another AceO

**Table 3** Final conformers for  $k$  calculation after  $\omega B97X-D3$  (Grid3) optimization and filtering.

System	Conformer type	Number
AceO	Reactant monomer	2
	TS monomer ( $\beta$ -scission)	2
	Reactant dimer	7
	TS dimer ( $\beta$ -scission)	3
	TS H-shift conformer	11
$\beta$ -ISOPO	Reactant monomer	8
	TS monomer ( $\beta$ -scission, hydroxymethyl side)	6
	Reactant dimer	25
	TS dimer ( $\beta$ -scission, hydroxymethyl side)	26
PhCH <sub>2</sub> O	Reactant monomer	1
	TS monomer (epoxy formation)	1
	Epoxy radical	1
	TS monomer (epoxy decomposition)	1
	Reactant dimer	3
	TS dimer (epoxy formation)	7
	Epoxy-PhCH <sub>2</sub> O complex	12
	TS dimer (epoxy decomposition) <sup>a</sup>	12
TS H-shift conformer	3	
PhC(O)O	Reactant monomer	1
	TS monomer ( $\beta$ -scission)	1
	Reactant dimer <sup>a</sup>	9
	TS dimer ( $\beta$ -scission) <sup>a</sup>	7

<sup>a</sup> The total number of conformers were counted after excluding the high-energy conformers which had a small imaginary frequency that could not be eliminated. (See Sections 3.3 and 3.4 for detailed discussions.)

in  ${}^3(AceO \cdots OAc)$  consistently increases the  $\beta$ -scission rate (see the  $k$  values in the same column of Table 4).

However, in contrast to the high theoretical  $k$  values, accretion products corresponding to the  $\beta$ -scission reaction (acetyl acetate,  $C_5H_8O_3$ ) were only observed at concentrations close to the detection limit in a recent experimental study<sup>18</sup>. Meanwhile, peroxide products ( $C_6H_{10}O_4$ ) corresponding to ISC were more abundant. The discrepancy between theoretical and experimental results implies that competing processes, rather than direct recombination on the triplet surface, may take place after the  $\beta$ -scission reaction. Our preliminary calculations on the  ${}^3(CH_3C(O) \cdots OAc)$  complex<sup>IV</sup> indicate that although recombination on the triplet surface is thermodynamically feasible, it is prevented by a substantial barrier (see Table S11). Thus, the formation of ROR'-type products likely requires an ISC after the  $\beta$ -scission.

For the intermolecular H-shift reaction, our  $k(DFT)$  values agree well with the reported value ( $8.85 \times 10^6 \text{ s}^{-1}$ <sup>14</sup>), while our  $k(CC)$  values are two orders of magnitude higher than the reported value ( $1.62 \times 10^3 \text{ s}^{-1}$ <sup>14</sup>). The lowest-energy TS H-shift conformer found by our conformer sampling workflow has lower  $E_{elzc}$  and  $G$  than that reported by Hasan et al.<sup>14</sup> (see Table S12),

<sup>IV</sup> This complex corresponds to the product complex of the  $\beta$ -scission reaction after ejecting the formaldehyde. The processes can be summarized as follows:  ${}^3(AceO \cdots OAc) \rightarrow {}^3(CH_3C(O) \cdots CH_2O \cdots OAc) \rightarrow {}^3(CH_3C(O) \cdots OAc) + CH_2O$



**Table 4** Rate coefficients of four alkoxy systems at 298.15 K. The  $k$  values were calculated at  $\omega$ B97X-D3 (Grid3) (labeled "DFT") and DLPNO-CCSD(T)-F12 (labeled "CC") levels using LC-TST (labeled "LC") and MC-TST (labeled "MC") methods, and are reported in  $s^{-1}$ .

System	Reaction Type	$\kappa_{\min}$ (DFT)	$\kappa_{\min}$ (CC)	$k_{LC}$ (DFT)	$k_{LC}$ (CC)	$k_{MC}$ (DFT)	$k_{MC}$ (CC)
AceO	$\beta$ -scission, free-radical	1.0	1.0	$2.33 \times 10^8$	$3.57 \times 10^9$	$2.33 \times 10^8$	$3.56 \times 10^9$
	$\beta$ -scission, in-complex	1.0	1.0	$1.65 \times 10^9$	$1.54 \times 10^{10}$	$6.40 \times 10^8$	$5.99 \times 10^9$
	Intermolecular H-shift	1.7	1.7	$8.91 \times 10^6$	$6.22 \times 10^5$	$1.29 \times 10^7$	$8.98 \times 10^5$
$\beta$ -ISOPO <sup>a</sup>	$\beta$ -scission, free-radical	1.2	1.2	$2.91 \times 10^9$	$7.44 \times 10^8$	$3.70 \times 10^9$	$9.47 \times 10^8$
	$\beta$ -scission, in-complex	1.1	1.1	$7.49 \times 10^{11}$	$6.46 \times 10^{11}$	$3.73 \times 10^{11}$	$3.22 \times 10^{11}$
PhCH <sub>2</sub> O	Epoxy formation, free-radical <sup>b</sup>	1.3	1.3	$1.19 \times 10^3$	$1.59 \times 10^4$	$1.19 \times 10^3$	$1.59 \times 10^4$
	Epoxy formation, in-complex	1.2	0.9	$2.93 \times 10^3$	$2.33 \times 10^4$	$3.13 \times 10^3$	$2.49 \times 10^4$
	Epoxy decomposition, free-radical <sup>b</sup>	1.7	1.7	$1.21 \times 10^6$	$1.29 \times 10^7$	$1.21 \times 10^6$	$1.29 \times 10^7$
	Epoxy decomposition, in-complex <sup>c</sup>	1.7	1.7	$7.19 \times 10^5$	$9.99 \times 10^6$	$5.40 \times 10^5$	$7.50 \times 10^6$
	Intermolecular H-shift	3.5	4.0	$6.79 \times 10^6$	$2.96 \times 10^6$	$6.30 \times 10^6$	$2.75 \times 10^6$
PhC(O)O	$\beta$ -scission, free-radical <sup>b</sup>	1.1 <sup>d</sup>	1.1 <sup>d</sup>	$1.97 \times 10^7$	$2.49 \times 10^8$	$1.97 \times 10^7$	$2.49 \times 10^8$
	$\beta$ -scission, in-complex <sup>c</sup>	1.1	1.0	$1.05 \times 10^7$	$1.32 \times 10^8$	$6.40 \times 10^6$	$8.02 \times 10^7$

<sup>a</sup> Only the  $\beta$ -scission reaction from the hydroxymethyl side is reported here ( $R_{m3.2.1}$  in Figure 3, see Section 3.2 for further discussions).

<sup>b</sup> The epoxy formation and decomposition reactions of PhCH<sub>2</sub>O<sup>\*</sup> and the  $\beta$ -scission reaction of PhC(O)O<sup>\*</sup> only have one conformer for each species. Thus, for these reactions  $k_{MC-TST} = k_{LC-TST}$ .

<sup>c</sup> High-energy dimers with a small imaginary frequency were excluded from  $k$  calculations (See Sections 3.3 and 3.4 for detailed discussions.).

<sup>d</sup> The reactant monomer obtained from IRC showed nonphysical imaginary frequencies after DFT optimization. Instead, a reactant monomer with the same geometry (RMSD = 0.09 Å) was used to calculate  $\kappa_{\min}$  values.

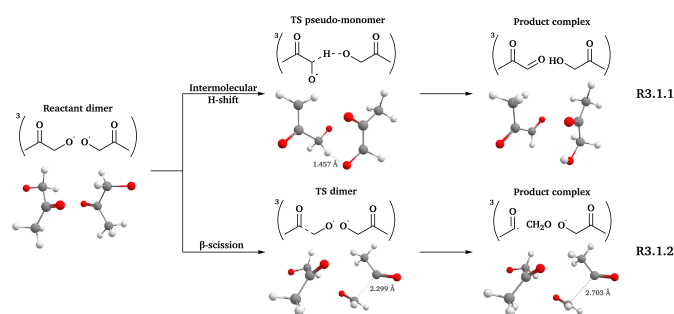


**Fig. 2** Reaction scheme of <sup>3</sup>(AceO...OAc). All 3D structures presented here are conformers with the lowest  $G$  after the  $\omega$ B97X-D3 (Grid3) optimization and filtering. Color coding: gray for C, white for H, and red for O.

suggesting that part of this variation may arise from different geometries used for CCSD(T) calculations. In addition, subtle differences in the CCSD(T) methods employed by the two studies may also contribute.

### 3.2 The $\beta$ -ISOPO system

The increased structural complexity of the  $\beta$ -ISOPO system leads to several possible pathways:  $\beta$ -scissions from the hydroxymethyl ( $R_{m3.2.1}$  in Figure 3), methyl ( $R_{m3.2.2}$  in Figure 3) and ethenyl ( $R_{m3.2.3}$  in Figure 3) sides; radical-double bond addition reactions at the  $\beta$  position (R3.2.2 (a) in Figure 3) and the  $\gamma$  position (R3.2.2 (b) in Figure 3). Intermolecular H-shift reactions are unlikely to occur, as no "aldehyde + alcohol" products can be formed for the <sup>3</sup>( $\beta$ -ISOPO... $\beta$ -ISOPO).

Given the expected large number of reaction channels and conformers of the  $\beta$ -ISOPO system, we first calculated the energy barriers ( $\Delta_b E_{elzc}$  and  $\Delta_b G$ , as defined in Table 2) of the following reactions, prior to comprehensive conformer sampling: three

$\beta$ -scission channels of isolated  $\beta$ -ISOPO<sup>\*</sup> ( $R_{m3.2.1}$ - $R_{m3.2.3}$ ), and two radical-double bond addition channels of the <sup>3</sup>( $\beta$ -ISOPO... $\beta$ -ISOPO) (R3.2.2 (a)-(b)). This step aimed to determine the energetically most favorable pathway, which was then selected for systematic conformer sampling. The barrier heights are listed in Table S13.

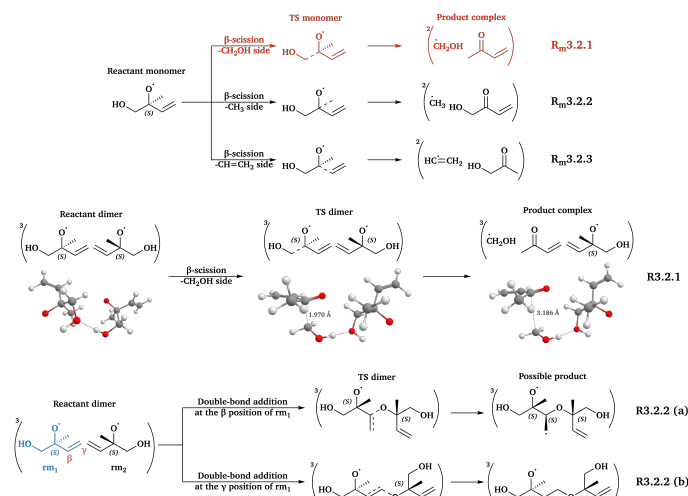


**Fig. 3** Reaction scheme of the  $\beta$ -ISOPO system. All 3D structures presented are the lowest- $G$  conformers, with the same level of theory and color coding as Figure 2.

As shown in Table S13,  $R_{m3.2.1}$  has significantly lower energy barriers than the other channels. The barrier heights of the three  $\beta$ -scission channels align with the trend of unimolecular RO<sup>\*</sup> reactions predicted by structure-activity relationship (SAR) models<sup>19</sup> ( $\Delta_b E_{elzc}(-CH_2OH) < \Delta_b E_{elzc}(-CH_3) < \Delta_b E_{elzc}(-CH=CH_2)$ ). Furthermore, differences among  $\Delta_b E_{elzc}$  and  $\Delta_b G$  values are large enough that the presence of another  $\beta$ -ISOPO<sup>\*</sup> is unlikely to change this conclusion. Thus, the systematic conformer sampling



workflow was applied only to  $\beta$ -scission reactions from the hydroxymethyl side (R<sub>m</sub>3.2.1 and R3.2.1 in Figure 3). The number of conformers and calculated  $k$  values are presented in Tables 3 and 4, respectively.

For R<sub>m</sub>3.2.1, our  $k(\text{CC})$  values ( $2.33 \times 10^8 \text{ s}^{-1}$ ) are around 10 times larger than the reported values ( $10^7 \text{ s}^{-1}$  at 300 K and 760 Torr)<sup>84,85</sup>. This discrepancy may result from different computational methods and kinetic models between earlier works and this study (e.g. B3LYP<sup>84,85</sup> and  $\omega$ B97X-D3, CCSD(T)<sup>84,85</sup> and DLPNO-CCSD(T)-F12, RRKM<sup>85</sup> and elementary TST, where in each pair the latter method is used in this study).

According to the first two sections in Table 4, the presence of another RO $\cdot$  in the  $^3(\text{RO} \cdots \text{OR})$  has a stronger impact on  $\beta$ -scission rates for the  $\beta$ -ISOPO system than for AceO. For  $\beta$ -ISOPO, the  $k(\text{in-complex})$  values are over two orders of magnitude higher than  $k(\text{free-radical})$ . We note that the  $\Delta_b G$  of R3.2.1 is only 1.30 kcal mol $^{-1}$  at the  $\omega$ B97X-D3 (Grid3) level, implying that elementary TST may not provide accurate  $k$  values<sup>86</sup>. Nevertheless, the notable difference in barrier heights ( $\Delta_b G(\text{free-radical, DFT}) - \Delta_b G(\text{in-complex, DFT}) = 3.34 \text{ kcal mol}^{-1}$ ) supports our qualitative conclusion: The in-complex  $\beta$ -scission reaction of  $\beta$ -ISOPO proceeds much faster than its free-radical counterpart.

### 3.3 The PhCH<sub>2</sub>O system

The  $\beta$ -scission reaction of isolated PhCH<sub>2</sub>O $\cdot$  has large energy barriers ( $\Delta_b E_{\text{elzc}} = 25.98 \text{ kcal mol}^{-1}$ ,  $\Delta_b G = 25.35 \text{ kcal mol}^{-1}$ ) at the  $\omega$ B97X-D3 (Grid3) level. Since the difference in  $\Delta_b E$  values between in-complex and free-radical reactions is typically less than 5 kcal mol $^{-1}$  (see Section S5 in SI), the  $\beta$ -scission channel is unlikely to be significant for  $^3(\text{PhCH}_2\text{O} \cdots \text{OCH}_2\text{Ph})$  as well. We then examined other possible free-radical reactions of PhCH<sub>2</sub>O $\cdot$  and proposed an epoxy formation-decomposition pathway (R3.3.2(1)-(2) in Figure 4). Similar epoxy formation-decomposition processes have been reported for unsaturated aliphatic RO $\cdot$ .<sup>22,87</sup> The conformer sampling workflow in Section 2 was applied to the species involved in epoxy formation-decomposition and intermolecular H-shift reactions.

Each monomer of the PhCH<sub>2</sub>O system (see Table 3) has only one conformer because of the rigid benzene ring. Thus,  $k(\text{MC-TST})$  equals to  $k(\text{LC-TST})$  for free-radical epoxy formation and decomposition reactions. Besides, one high-energy TS dimer of the epoxy decomposition reaction showed a second small imaginary frequency ( $-8.39 \text{ cm}^{-1}$ ), which could not be eliminated by the Grid3 optimization or manual displacements as described in Section 2.3. This conformer was therefore excluded from the  $k$  calculation.

Table 4 summarizes the  $k$  values for the free-radical and in-complex reactions of the PhCH<sub>2</sub>O system. Compared to earlier studies<sup>22,87</sup>, the epoxy formation reaction shows a larger energy barrier in isolated PhCH<sub>2</sub>O $\cdot$  ( $\Delta_b E_{\text{elzc}}(\text{CC, this study}) = 12.86 \text{ kcal mol}^{-1}$ ) than in aliphatic RO $\cdot$  ( $\Delta_b E(\text{coupled cluster, earlier studies}) = 4.60^{22} - 9.5^{87} \text{ kcal mol}^{-1}$ ). This gap is significant regardless of the different coupled cluster methods applied. We further examined their reaction energies ( $\Delta_r E$ , defined in Table 2). The epoxy

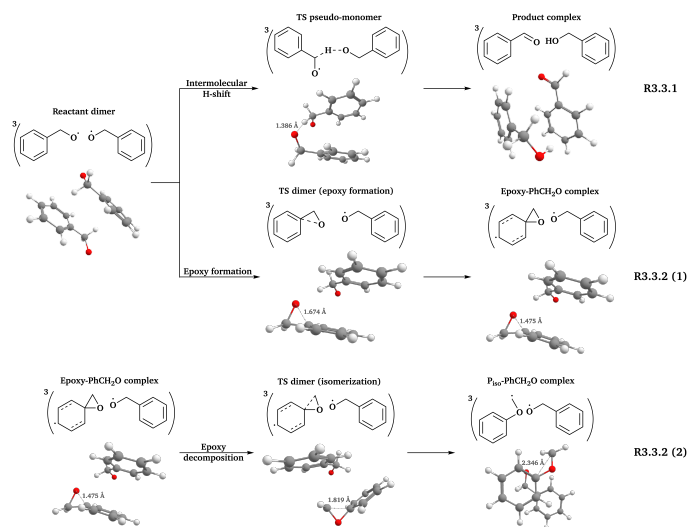


**Fig. 4** Reaction scheme of the PhCH<sub>2</sub>O system. All 3D structures presented are the lowest- $G$  conformers, with the same level of theory and color coding as Figure 2.

formation reaction in aliphatic RO $\cdot$  is isoergic or slightly endoergic ( $\Delta_r E(\text{coupled cluster, earlier studies}) = -0.66 - 2.23 \text{ kcal mol}^{-1}$ <sup>22</sup>), while in PhCH<sub>2</sub>O $\cdot$  it is much more endoergic ( $\Delta_r E_{\text{elzc}}(\text{CC}) = 10.27 \text{ kcal mol}^{-1}$ ), and therefore, thermodynamically less favorable.

Although the epoxy decomposition channel has  $k$  values comparable to intermolecular H-shift, its contribution is not expected to exceed 1% of the final products. This is because its prerequisite step, epoxy formation, proceeds around two orders of magnitude more slowly than the intermolecular H-shift (see Table 4).

Unlike the two systems in Sections 3.1 and 3.2, the presence of another PhCH<sub>2</sub>O $\cdot$  does not exhibit a consistent effect on the reactions of  $^3(\text{PhCH}_2\text{O} \cdots \text{OCH}_2\text{Ph})$ : It slightly increases the  $k$  values of epoxy formation, but decreases those of epoxy decomposition (see Table 4).

### 3.4 The PhC(O)O system

Due to the structural constraints of PhC(O)O $\cdot$ , only the  $\beta$ -scission channel (see Figure 5) is feasible for this system, and the number of conformers is relatively small (see Table 3). Similar to the PhCH<sub>2</sub>O system, one high-energy reactant dimer and two high-energy TS dimers of the  $\beta$ -scission in  $^3(\text{PhC}(\text{O})\text{O} \cdots \text{O}(\text{O})\text{Ph})$  showed small imaginary frequencies that could not be eliminated after using the techniques in Section 2.3. Thus, these three conformers were not included when calculating  $k$ .

As shown in Table 4, free-radical and in-complex  $\beta$ -scission reactions are relatively fast for the PhC(O)O system. The presence of another PhC(O)O $\cdot$  in the complex increases  $k(\text{CC})$  while decreasing  $k(\text{DFT})$ . However, based on previous studies of CH<sub>3</sub>C(O)O $\cdot$ <sup>88,89</sup>, the CO<sub>2</sub> ejection transition state likely has substantial multireference characters, suggesting that neither  $k(\text{DFT})$  nor  $k(\text{CC})$  is particularly accurate.



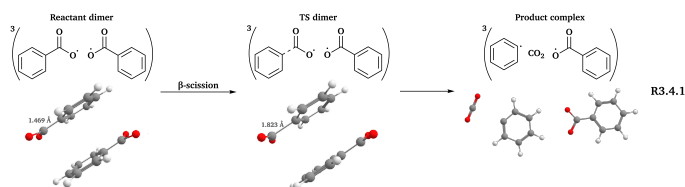


**Fig. 5** Reaction scheme of the PhC(O)O system. All 3D structures presented are the lowest- $G$  conformers, with the same level of theory and color coding as Figure 2.

$$p(d/m) = \frac{k_{LC}(\text{in-complex, CC})}{k_{LC}(\text{free-radical, CC})} \quad (3)$$

$$p(\text{MC/LC}) = \frac{k_{MC}(\text{in-complex, CC})}{k_{LC}(\text{in-complex, CC})} \quad (4)$$

$$p(\text{CC/DFT}) = \frac{k_{LC}(\text{in-complex, CC})}{k_{LC}(\text{in-complex, DFT})} \quad (5)$$

**Table 5** Results of  $p(d/m)$ ,  $p(\text{MC/LC})$  and  $p(\text{CC/DFT})$ . Parameters were calculated using Equations 3, 4 and 5, respectively. Definitions of  $k(\text{DFT})$  and  $k(\text{CC})$  are explained in Table 2.

System and reaction	$p(d/m)$	$p(\text{MC/LC})$	$p(\text{CC/DFT})$
AceO, $\beta$ -scission	4.33	0.39	9.35
AceO, Intermolecular H-shift	—	1.44	0.07
$\beta$ -ISOPO, $\beta$ -scission	868.81	0.50	0.86
PhCH <sub>2</sub> O, Epoxy formation	1.46	1.07	7.96
PhCH <sub>2</sub> O, Epoxy decomposition	0.77	0.75	13.89
PhCH <sub>2</sub> O, Intermolecular H-shift	—	0.93	0.44
PhC(O)O, $\beta$ -scission	0.53	0.61	12.52

### 3.5 General findings of the four systems

We plotted the range of  $k$  for  $\beta$ -scission reactions in AceO,  $\beta$ -ISOPO and PhC(O)O systems, as shown in Figure 6. The  $\beta$ -scission reaction is kinetically unfeasible for the PhCH<sub>2</sub>O system and is thus not included in the figure.

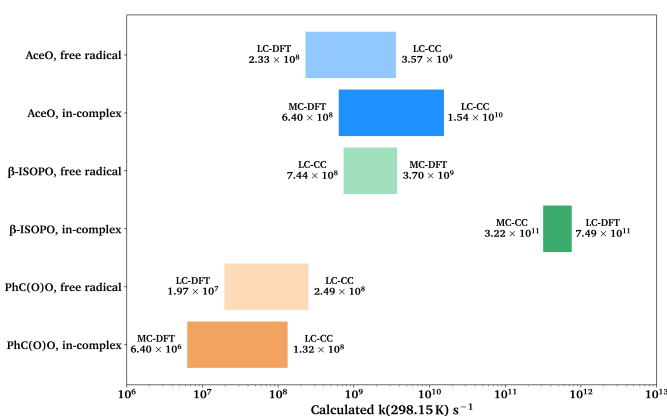


**Fig. 6** The range of free-radical and in-complex  $\beta$ -scission reactions of different systems. The origin of the x-axis is set to 10<sup>6</sup> s<sup>-1</sup>. Acronyms: MC for MC-TST, LC for LC-TST, DFT for  $\omega$ B97X-D3 (Grid3), CC for DLPNO-CCSD(T)-F12.

From Figure 6, the in-complex  $\beta$ -scission reaction roughly follows the trend  $k(\beta\text{-ISOPO}) > k(\text{AceO}) > k(\text{PhC(O)O})$ , which is consistent with the SAR-predicted order of unimolecular RO<sup>•</sup> reactions<sup>19,87</sup>. While Figure 6 shows the overall magnitude of  $k$  for  $\beta$ -scission reactions, we also evaluate factors that influence the calculated  $k$  values of all studied reaction channels. These factors include: (1) The reaction takes place in <sup>3</sup>(RO<sup>•</sup>···OR) or in isolated RO<sup>•</sup>. (2) The  $k$  was calculated using MC-TST or LC-TST methods. (3) The  $\Delta_b G$  values were calculated at  $\omega$ B97X-D3 (Grid3) or DLPNO-CCSD(T)-F12 levels of theory.

To quantify the effects of those factors on  $k$ , we defined three parameters:  $p(d/m)$ ,  $p(\text{MC/LC})$  and  $p(\text{CC/DFT})$ . For computing  $p(d/m)$  (Equation 3) and  $p(\text{CC/DFT})$  (Equation 5), only  $k(\text{LC-TST})$  values are used to eliminate the effect of multiple conformers. Since intermolecular H-shift reactions involves two RO<sup>•</sup> in the <sup>3</sup>(RO<sup>•</sup>···OR) complex,  $p(d/m)$  does not apply to them.  $p(\text{MC/LC})$  reflects the effects of multiple conformers and is computed using only  $k(\text{in-complex})$  values. For some free-radical reactions, there is only one conformer for each species (see Table 3), and consequently, their  $p(\text{MC/LC})$  always equals to 1. Calculated  $p$  values are listed in Table 5.

According to Tables 4 and 5, the formation of <sup>3</sup>(RO<sup>•</sup>···OR) significantly increases the  $\beta$ -scission rates of aliphatic systems. In particular, the presence of the other  $\beta$ -ISOPO<sup>•</sup> raises the  $k(\beta\text{-scission})$  by a factor of 868 at the DLPNO-CCSD(T)-F12 level. This increase possibly results from an intermolecular hydrogen bond that stabilizes the TS dimer (O<sub>3</sub>-H<sub>12</sub>···O<sub>1</sub> in Figure S2 b). Although the TS monomer also has a hydrogen bond (O<sub>1</sub>-H<sub>3</sub>···O<sub>2</sub> in Figure S2 a), it is much weaker compared to its counterpart in the TS dimer: The O<sup>•</sup>···H distance is longer (2.4 Å vs. 1.7 Å in the TS dimer), and the O-H···O angle is less favorable (103° vs. 177° in the TS dimer).

In addition, the binding energy of <sup>3</sup>(RO<sup>•</sup>···OR) may also affect  $p(d/m)$  values. For example, the <sup>3</sup>( $\beta$ -ISOPO<sup>•</sup>··· $\beta$ -ISOPO) is among the strongest-bound complexes ( $D_{\text{elzc}}(\text{DFT}) = 7.96 \text{ kcal mol}^{-1}$ ,  $D_{\text{elzc}}(\text{CC}) = 6.52 \text{ kcal mol}^{-1}$ ; see Table S2), and its  $p(d/m)$  is exceptionally large. However, the other three complexes have similar binding energies (within 6 – 8 kcal mol<sup>-1</sup>, see Table S2), while their  $p(d/m)$  values are between 0.5 and 5. This observation suggests that while the binding energy may contribute to differences between  $k(\text{in-complex})$  and  $k(\text{free-radical})$ , it is unlikely to be the determining factor.

$p(\text{MC/LC})$  depends on the relative number of low-energy TS and reactant conformers (see Table 3). For example, the intermolecular H-shift reaction of <sup>3</sup>(AceO<sup>•</sup>···OAce) has 11 low-energy TS conformers, leading to  $p(\text{MC/LC}) > 1$ . However, all  $p(\text{MC/LC})$  values are between 0.3 – 1.5, indicating that multiple conformers change the  $k$  value by less than a factor of three. Thus, the multi-conformer effects are a relatively minor source of error, as long as the global minimum conformers (with lowest  $G$ ) have been correctly identified by the sampling workflow.

$p(\text{CC/DFT})$  is an indicator of consistency between  $k(\text{DFT})$  and  $k(\text{CC})$  values. If the difference between DFT and CCSD(T) results were consistent and systematic among the four systems, the four  $p(\text{CC/DFT})$  values could be expected to be similar. However,  $p(\text{CC/DFT})$  varies from 0.07 to 12.54 (see Table 5). Notably, the



two H-shift reactions have  $p(\text{CC/DFT}) < 1$ , while the  $\beta$ -scission reactions have  $p(\text{CC/DFT})$  values close to or above one. Considering the typical uncertainties when applying DFT and CCSD(T) methods to complex open-shell systems, the disagreement shown in Table 5 is within an acceptable range.

## 4 Conclusions

Based on previous studies<sup>14,15,31</sup>, we developed a systematic conformer sampling workflow for the key intermediate in  $\text{RO}_2^*$  recombination reactions,  $^3(\text{RO} \cdots \text{OR})$ . This workflow was applied to four representative alkoxy systems in the atmosphere: AceO,  $\beta$ -ISOPO,  $\text{PhCH}_2\text{O}$  and  $\text{PhC}(\text{O})\text{O}$ . Rate coefficients for typical reactions were computed at  $\omega\text{B97X-D3/ma-def2-TZVP}$  (Grid3) and UHF-DLPNO-CCSD(T)-F12/cc-pVDZ-F12 levels of theory.

We examined the established channels of these systems, including  $\beta$ -scission and intermolecular H-shift reactions. Our workflow improved the conformer sampling especially for intermolecular H-shift reactions. For example, we identified a lower-energy TS dimer for the  $\beta$ -scission of  $^3(\text{AceO} \cdots \text{OAce})$ , compared to the best TS conformer reported previously<sup>14</sup>. Furthermore, we investigated two novel pathways:  $\text{RO}^*$  addition to the double bond of the other  $\text{RO}^*$  in the complex (R3.2.2(a)-(b) in Figure 3), and epoxy formation-decomposition of  $\text{PhCH}_2\text{O}^*$ , leading to a phenoxymethyl radical (R3.3.2(1)-(2) in Figure 4). However, neither novel pathway was competitive compared to in-complex  $\beta$ -scission and intermolecular H-shift reactions (see Table 4).

Our conformer sampling workflow was tested and found to be robust for both aliphatic and aromatic systems. Including multiple conformers in  $k$  calculations has a modest effect (less than a factor of three, see Table 5), provided that the lowest-energy conformers have been correctly identified. On the other hand, CCSD(T) energy corrections influence  $k$  values by less than a factor of 15 (see Table 5). Interestingly, our CCSD(T) corrections tend to slow down intermolecular H-shift reactions, while accelerating  $\beta$ -scission reactions (see Table 5).

For  $\beta$ -scission reactions in the other three alkoxy systems, the  $k(\text{in-complex})$  and  $k(\text{free-radical})$  values are comparable. However, in the  $\beta$ -ISOPO system, the  $k(\text{in-complex})$  is two orders of magnitude higher than  $k(\text{free-radical})$ . This rate enhancement is likely due to the intermolecular hydrogen bond that stabilizes the transition state (see Figure S2).

Our observations on  $k$  values tentatively suggest that for  $\beta$ -scission reactions,  $k(\text{free-radical})$  can constrain the lower limit of  $k(\text{in-complex})$ , as well as estimate the order-of-magnitude for  $k(\text{in-complex})$  in relatively simple or weakly-bound systems. However, for aerosol-relevant systems with H-bonding functional groups,  $k(\text{in-complex})$  may be significantly enhanced. This may help explain the substantial ester formation detected in  $\alpha$ -pinene ozonolysis<sup>17</sup>.

## Author contributions

- Hongye Fraise Zhao: Investigation (main), Methodology (main), Formal analysis, Writing – original draft.
- Lauri Franzon: Investigation (support), Methodology (support), Supervision (support), Writing – review & editing (support).

- Severi Juttula: Software (support), Writing – review & editing (support).
- Robert Skog: Methodology (support), Writing – review & editing (support).
- Theo Kurtén: Project administration, Funding acquisition, Resources, Supervision (main), Writing – review & editing (main).
- Nanna Myllys: Funding acquisition, Supervision (support), Writing – review & editing (support).

## Conflicts of interest

There are no conflicts to declare.

## Data availability

Supplementary Information (SI) files are available. The attached SI.pdf contains data supporting the findings in this article. Detailed ORCA output files (in .out format) and  $\omega\text{B97X-D3}$  (Grid3)-optimized structures (in .xyz format) of all conformers, which contain necessary information (e.g. frequencies, energy values) for  $k$  calculations, are published in the Zenodo archive [DOI: 10.5281/zenodo.19210535].

## Acknowledgements

We gratefully acknowledge the Oskar Öflunds Stiftelse for awarding the 2025 scientific research grant that supported this project. We also acknowledge funding from the Research Council of Finland (Center of Excellence Virtual Laboratory for Molecular Level Atmospheric Transformations (VILMA) grant no. 346369 and Academy Research Fellowship grant no. 347775) and European Union (ERC project AtmosCOC no. 101161989).

In addition, we acknowledge the CSC-IT Center for Science Ltd. (CSC) of Finland for providing the high-performance computing (HPC) environment and technical assistance. We also acknowledge the support from the Doctoral Program in Chemistry and Molecular Sciences (CHEMS-DP) at the University of Helsinki.

## Notes and references

- 1 K. Vohra, A. Vodonos, J. Schwartz, E. A. Marais, M. P. Sulprizio and L. J. Mickley, *Environmental research*, 2021, **195**, 110754.
- 2 T. Muenzel, M. Sørensen, O. Hahad, M. Nieuwenhuijsen and A. Daiber, *Nature Reviews Cardiology*, 2023, **20**, 651–669.
- 3 U. Pöschl, *Angewandte Chemie International Edition*, 2005, **44**, 7520–7540.
- 4 A. P. Tsimpidi, S. Scholz, A. Milousis, N. Mihalopoulos and V. A. Karydis, *Atmospheric Chemistry and Physics*, 2025, **25**, 10183–10213.
- 5 H. Wang, X. Liu, C. Wu and G. Lin, *Atmospheric Chemistry and Physics*, 2024, **24**, 3309–3328.
- 6 Z. He, X. Wang, Z. Ling, J. Zhao, H. Guo, M. Shao and Z. Wang, *Atmospheric Chemistry and Physics*, 2019, **19**, 8801–8816.
- 7 J. J. Orlando and G. S. Tyndall, *Chemical Society Reviews*, 2012, **41**, 6294–6317.



- 8 K. C. Barsanti and J. F. Pankow, *Atmospheric Environment*, 2004, **38**, 4371–4382.
- 9 J. H. Kroll and J. H. Seinfeld, *Atmospheric Environment*, 2008, **42**, 3593–3624.
- 10 S. E. Murphy, J. D. Crouse, K. H. Møller, S. P. Rezgui, N. J. Hafeman, J. Park, H. G. Kjaergaard, B. M. Stoltz and P. O. Wennberg, *Environmental Science: Atmospheres*, 2023, **3**, 882–893.
- 11 V.-T. Salo, R. Valiev, S. Lehtola and T. Kurtén, *The Journal of Physical Chemistry A*, 2022, **126**, 4046–4056.
- 12 G. Ghigo, A. Maranzana and G. Tonachini, *The Journal of chemical physics*, 2003, **118**, 10575–10583.
- 13 L. Franzon, *The Journal of Physical Chemistry A*, 2023, **127**, 5956–5966.
- 14 G. Hasan, V.-T. Salo, R. R. Valiev, J. Kubečka and T. Kurtén, *The Journal of Physical Chemistry A*, 2020, **124**, 8305–8320.
- 15 G. Hasan, V.-T. Salo, T. Golin Almeida, R. R. Valiev and T. Kurtén, *The Journal of Physical Chemistry A*, 2023, **127**, 1686–1696.
- 16 R. R. Valiev, G. Hasan, V.-T. Salo, J. Kubečka and T. Kurtén, *The Journal of Physical Chemistry A*, 2019, **123**, 6596–6604.
- 17 O. Peräylä, T. Berndt, L. Franzon, G. Hasan, M. Meder, R. R. Valiev, C. D. Daub, J. G. Varelas, F. M. Geiger, R. J. Thomson *et al.*, *Journal of the American Chemical Society*, 2023, **145**, 7780–7790.
- 18 B. N. Frandsen, L. Franzon, M. Meder, D. Pasik, E. Ahongshangbam, N. Vinkvist, N. Myllys, S. Iyer, M. P. Rissanen, M. Ehn *et al.*, *ACS Earth and Space Chemistry*, 2025.
- 19 L. Vereecken and J. Peeters, *Physical Chemistry Chemical Physics*, 2009, **11**, 9062–9074.
- 20 L. Vereecken and J. Peeters, *Physical Chemistry Chemical Physics*, 2010, **12**, 12608–12620.
- 21 L. Franzon, M. Camredon, R. Valorso, B. Aumont and T. Kurtén, *Atmospheric Chemistry and Physics*, 2024, **24**, 11679–11699.
- 22 V. S. Nguyen and J. Peeters, *The Journal of Physical Chemistry A*, 2015, **119**, 7270–7276.
- 23 L. Vereecken, P. Carlsson, A. Novelli, F. Bernard, S. Brown, C. Cho, J. Crowley, H. Fuchs, W. Mellouki, D. Reimer *et al.*, *Physical Chemistry Chemical Physics*, 2021, **23**, 5496–5515.
- 24 J. J. Orlando, G. S. Tyndall and T. J. Wallington, *Chemical reviews*, 2003, **103**, 4657–4690.
- 25 I. Mandal, C. D. Daub, R. Valiev, T. Kurtén and R. B. Gerber, *Physical Chemistry Chemical Physics*, 2025, **27**, 2395–2404.
- 26 B. Nozière and R. Patrick, *Science Advances*, 2026, **12**, eaeb6495.
- 27 S. Grimme, C. Bannwarth and P. Shushkov, *Journal of chemical theory and computation*, 2017, **13**, 1989–2009.
- 28 C. Bannwarth, S. Ehlert and S. Grimme, *Journal of chemical theory and computation*, 2019, **15**, 1652–1671.
- 29 S. Spicher and S. Grimme, *Angewandte Chemie International Edition*, 2020, **59**, 15665–15673.
- 30 International Union of Pure and Applied Chemistry (IUPAC), *conformer*, <https://doi.org/10.1351/goldbook.C01262>, 2025.
- 31 K. H. Møller, R. V. Otkjær, N. Hyttinen, T. Kurtén and H. G. Kjaergaard, *The Journal of Physical Chemistry A*, 2016, **120**, 10072–10087.
- 32 Q. Zhao, K. H. Møller, J. Chen and H. G. Kjaergaard, *The Journal of Physical Chemistry A*, 2022, **126**, 6483–6494.
- 33 D. Ferro-Costas, E. Martinez-Nunez, J. Rodriguez-Otero, E. Cabaleiro-Lago, C. M. Estévez, B. Fernandez, A. Fernandez-Ramos and S. A. Vazquez, *The Journal of Physical Chemistry A*, 2018, **122**, 4790–4800.
- 34 T. Berndt, W. Scholz, B. Mentler, L. Fischer, H. Herrmann, M. Kulmala and A. Hansel, *Angewandte Chemie International Edition*, 2018, **57**, 3820–3824.
- 35 K. Zuraski, F. J. Grieman, A. O. Hui, J. Cowen, F. A. Winiberg, C. J. Percival, M. Okumura and S. P. Sander, *The Journal of Physical Chemistry A*, 2023, **127**, 7772–7792.
- 36 P. O. Wennberg, K. H. Bates, J. D. Crouse, L. G. Dodson, R. C. McVay, L. A. Mertens, T. B. Nguyen, E. Praske, R. H. Schwantes, M. D. Smarte *et al.*, *Chemical reviews*, 2018, **118**, 3337–3390.
- 37 R. Wu, S. Pan, Y. Li and L. Wang, *The Journal of Physical Chemistry A*, 2014, **118**, 4533–4547.
- 38 B. Feng, C. Sun and S. Zhang, *Atmospheric Environment*, 2019, **201**, 18–27.
- 39 Y. Ren, L. Zhou, A. Mellouki, V. Daële, M. Idir, S. S. Brown, B. Ruscic, R. S. Paton, M. R. McGillen and A. R. Ravishankara, *Atmospheric Chemistry and Physics*, 2021, **21**, 13537–13551.
- 40 Wavefunction Inc., *SPARTAN'24*, <https://www.wavefun.com/spartan>, 2024, Accessed August 2025.
- 41 J. Zhang and M. Dolg, *Physical Chemistry Chemical Physics*, 2015, **17**, 24173–24181.
- 42 J. Zhang and M. Dolg, *Physical Chemistry Chemical Physics*, 2016, **18**, 3003–3010.
- 43 B. de Souza, *Angewandte Chemie International Edition*, 2025, **64**, e202500393.
- 44 F. Neese, *WIREs Computational Molecular Science*, 2025, **15**, e70019.
- 45 C. Bannwarth, E. Caldeweyher, S. Ehlert, A. Hansen, P. Pracht, J. Seibert, S. Spicher and S. Grimme, *Wiley Interdisciplinary Reviews: Computational Molecular Science*, 2021, **11**, e1493.
- 46 S. Grimme *et al.*, *XTB version 6.7.1*, GitHub repository, 2024, <https://github.com/grimme-lab/xtb/releases/tag/v6.7.1>, Accessed August 2025.
- 47 J. Kubečka, V. Besel, T. Kurtén, N. Myllys and H. Vehkamäki, *J. Phys. Chem. A*, 2019, **123**, 6022–6033.
- 48 J. Kubečka, A. S. Christensen, F. R. Rasmussen and J. Elm, *Environ. Sci. Technol. Lett.*, 2022, **9**, 239–244.
- 49 J. Kubečka, *JKCS2.1: Jammy Key for Configurational Sampling*, <https://github.com/kubeckaj/JKCS2.1>, 2024, Accessed August 2025.
- 50 International Union of Pure and Applied Chemistry (IUPAC), *elementary reaction*, <https://doi.org/10.1351/goldbook.E02035>, 2025.
- 51 H. Eyring, *The Journal of chemical physics*, 1935, **3**, 107–115.
- 52 K. J. Laidler and M. C. King, *J. phys. Chem*, 1983, **87**, 2657–



- 2664.
- 53 L. Vereecken and J. Peeters, *The Journal of chemical physics*, 2003, **119**, 5159–5170.
- 54 C. Eckart, *Physical Review*, 1930, **35**, 1303.
- 55 K. Ishida, K. Morokuma and A. Komornicki, *The Journal of Chemical Physics*, 1977, **66**, 2153–2156.
- 56 A. D. Becke, *The Journal of chemical physics*, 1993, **98**, 5648–5652.
- 57 C. Lee, W. Yang and R. G. Parr, *Physical review B*, 1988, **37**, 785.
- 58 J. Zheng, X. Xu and D. G. Truhlar, *Theoretical Chemistry Accounts*, 2011, **128**, 295–305.
- 59 F. Weigend and R. Ahlrichs, *Physical Chemistry Chemical Physics*, 2005, **7**, 3297–3305.
- 60 J.-D. Chai and M. Head-Gordon, *Physical Chemistry Chemical Physics*, 2008, **10**, 6615–6620.
- 61 Y.-S. Lin, G.-D. Li, S.-P. Mao and J.-D. Chai, *Journal of Chemical Theory and Computation*, 2013, **9**, 263–272.
- 62 L. Goerigk, A. Hansen, C. Bauer, S. Ehrlich, A. Najibi and S. Grimme, *Physical Chemistry Chemical Physics*, 2017, **19**, 32184–32215.
- 63 J. Elm, J. Kubečka, V. Besel, M. J. Jääskeläinen, R. Halonen, T. Kurtén and H. Vehkamäki, *Journal of Aerosol Science*, 2020, **149**, 105621.
- 64 H. Zhao, *Rapid alkoxy radical  $\beta$ -scission in bimolecular complexes*, 2024, <http://hdl.handle.net/10138/589458>.
- 65 N. Myllys, J. Elm and T. Kurtén, *Computational and Theoretical Chemistry*, 2016, **1098**, 1–12.
- 66 B. Helmich-Paris, B. de Souza, F. Neese and R. Izsák, *The Journal of Chemical Physics*, 2021, **155**, 104109.
- 67 F. Neese *et al.*, *ORCA 6.0 Manual Section 7.3. Details on the numerical integration grids*, 2024, <https://www.faccts.de/docs/orca/6.0/manual/contents/detailed/numint.html>, Accessed November 2025.
- 68 S. P. Sitkiewicz, R. Zaleśny, E. Ramos-Cordoba, J. M. Luis and E. Matito, *The Journal of Physical Chemistry Letters*, 2022, **13**, 5963–5968.
- 69 J. A. Pople and R. K. Nesbet, *The Journal of Chemical Physics*, 1954, **22**, 571–572.
- 70 C. Riplinger, B. Sandhoefer, A. Hansen and F. Neese, *The Journal of Chemical Physics*, 2013, **139**, 134101.
- 71 F. Pavošević, F. Neese and E. F. Valeev, *The Journal of Chemical Physics*, 2014, **141**, 054106.
- 72 K. A. Peterson, T. B. Adler and H.-J. Werner, *The Journal of Chemical Physics*, 2008, **128**, 084102.
- 73 D. G. Liakos, M. Sparta, M. K. Kesharwani, J. M. Martin and F. Neese, *Journal of chemical theory and computation*, 2015, **11**, 1525–1539.
- 74 R. A. Kendall, T. H. Dunning Jr and R. J. Harrison, *The Journal of chemical physics*, 1992, **96**, 6796–6806.
- 75 T. H. Dunning Jr, *The Journal of chemical physics*, 1989, **90**, 1007–1023.
- 76 G. Schmitz and J. Elm, *ACS omega*, 2020, **5**, 7601–7612.
- 77 R. B. Best, X. Zhu, J. Shim, P. E. Lopes, J. Mittal, M. Feig and A. D. MacKerell Jr, *Journal of chemical theory and computation*, 2012, **8**, 3257–3273.
- 78 A. D. M. Jr. *et al.*, *CHARMM Force Fields*, [http://mackerell1.umd.edu/charmm\\_ff.shtml](http://mackerell1.umd.edu/charmm_ff.shtml), 2025, Accessed August 2025.
- 79 E. D. Glendening, J. K. Badenhop, A. E. Reed, J. E. Carpenter, J. A. Bohmann, C. M. Morales, P. Karafiloglou, C. R. Landis and F. Weinhold, *NBO 7.0*, 2018, Version 7.0.10 (8-Feb-2021), Theoretical Chemistry Institute, University of Wisconsin, Madison, WI.
- 80 E. D. Glendening, C. R. Landis and F. Weinhold, *Journal of computational chemistry*, 2019, **40**, 2234–2241.
- 81 H. Wu, M. Engsvang, Y. Knattrup, J. Kubečka and J. Elm, *ACS omega*, 2023, **8**, 45065–45077.
- 82 Y. Knattrup, J. Kubečka, H. Wu, F. Jensen and J. Elm, *RSC advances*, 2024, **14**, 20048–20055.
- 83 F. Neese *et al.*, *ORCA 6.0 Manual Section 6.3.6: Constrained Optimizations*, 2024, <https://www.faccts.de/docs/orca/6.0/manual/contents/typical/optimizations.html#constrained-optimizations>, Accessed August 2025.
- 84 W. Lei and R. Zhang, *The Journal of Physical Chemistry A*, 2001, **105**, 3808–3815.
- 85 J. Park, J. C. Stephens, R. Zhang and S. W. North, *The Journal of Physical Chemistry A*, 2003, **107**, 6408–6414.
- 86 J. L. Bao and D. G. Truhlar, *Chemical Society Reviews*, 2017, **46**, 7548–7596.
- 87 A. Novelli, C. Cho, H. Fuchs, A. Hofzumahaus, F. Rohrer, R. Tillmann, A. Kiendler-Scharr, A. Wahner and L. Vereecken, *Physical Chemistry Chemical Physics*, 2021, **23**, 5474–5495.
- 88 C. M. Rosado-Reyes and J. S. Francisco, *The Journal of Physical Chemistry A*, 2006, **110**, 4419–4433.
- 89 Y. Z. Zhou, S. Li, Q. S. Li and S. W. Zhang, *Journal of Molecular Structure: THEOCHEM*, 2008, **854**, 40–45.

## Data Availability Statement for

### Clustering effects on the reactivity of alkoxy radicals: Rate coefficients of $^3(\text{RO}\cdots\text{OR})$ complexes accounting for multiple conformers

Hongye Fraise Zhao<sup>†</sup>, Lauri Franzon<sup>†</sup>, Severi Juttula<sup>†</sup>, Robert Skog<sup>†</sup>, Nanna Myllys<sup>†</sup> and Theo Kurtén<sup>†\*</sup>

<sup>†</sup>*Department of Chemistry, University of Helsinki, A.I. Virtasen aukio 1 (Chemicum), 00560, Helsinki, Finland.*

<sup>\*</sup>*E-mail: theo.kurten@helsinki.fi*

Supplementary Information (SI) files are available. The attached SI.pdf contains data supporting the findings in this article. Detailed ORCA output files (in .out format) and ωB97X-D3 (Grid3)-optimized structures (in .xyz format) of all conformers, which contain necessary information (e.g. frequencies, energy values) for  $k$  calculations, are published in the Zenodo archive [DOI: 10.5281/zenodo.19210535].

Note: The Zenodo archive is not yet publicly visible. Its pre-publication version can be accessed and downloaded via: [https://zenodo.org/records/19210535?preview=1&token=eyJhbGciOiJIUzUxMiJ9.eyJpZCI6ImY0Njg5NDNjLTE5NzctNDY4OC1hNGNmLThjYWJjZDA0Y2NiZCI6ImRhdGEiOnt9LCJyYW5kb20iOiJmYjQwY2Y1YmQxZmQxZTE0ZjAxODQ3ZTAyYTNjNTlkMCI9.2QJGib2uEiSsddXVGyTsBD6TQys96KT16xeIOA1121P5MglxBNjYr\\_ik7ErWnKqQxY2Ve4km9VT6A576jazcFw](https://zenodo.org/records/19210535?preview=1&token=eyJhbGciOiJIUzUxMiJ9.eyJpZCI6ImY0Njg5NDNjLTE5NzctNDY4OC1hNGNmLThjYWJjZDA0Y2NiZCI6ImRhdGEiOnt9LCJyYW5kb20iOiJmYjQwY2Y1YmQxZmQxZTE0ZjAxODQ3ZTAyYTNjNTlkMCI9.2QJGib2uEiSsddXVGyTsBD6TQys96KT16xeIOA1121P5MglxBNjYr_ik7ErWnKqQxY2Ve4km9VT6A576jazcFw)

